



ELSEVIER

Characterization of CsI photocathodes for use in a fast RICH detector

C. Lu, Z. Cheng, K.T. McDonald*, D.R. Marlow, E.J. Prebys, R.L. Wixted

Joseph Henry Laboratories, Princeton University, Princeton, NJ 08544, USA

Received 2 May 1995

Abstract

We have completed a series of measurements that provide a basic understanding of the properties of CsI photocathodes for use in ring imaging Cherenkov (RICH) detectors. The quantum efficiency of CsI has been measured relative to an NIST-calibrated photodiode and is in excellent agreement with a similar measurement by Breskin et al. A representative value of the quantum efficiency is 20% at 180 nm. The quantum efficiency of a fresh photocathode is unaffected by temperature, but heating the photocathode can be helpful if it has been exposed to water vapor, or has been aged by a large integrated photocurrent. Detailed studies of aging show a “fast” component that appears to be associated with a rise in the work function, and a “slow” component associated with conversion of the bulk CsI to Cs. We judge that a practical lifetime of a CsI photocathode is until it has lost 20% of its initial quantum efficiency, which process is dominated by the “fast” rise in the work function. This rise occurs both due to photoelectron transport with an effective lifetime of $0.1 \mu\text{C}/\text{mm}^2$ and due to positive-ion bombardment with an effective lifetime of $15 \mu\text{C}/\text{mm}^2$. When the CsI photocathode is used in a chamber with gas gain greater than 150 the latter lifetime is the relevant one. This lifetime should be sufficient for use of a RICH detector at an e^+e^- B factory. The reduction of quantum efficiency of a CsI photocathode in a gas-filled chamber has been studied for several gases over a wide range of reduced electric field. This effect can be minimized by use of atmospheric-pressure methane in a chamber with anode wires rather than a mesh. We have also demonstrated that excellent spatial resolution for the location of the photoelectrons can be obtained using a coarse cathode-pad readout if the anode–cathode spacing is similar to the pad width.

1. Introduction and summary

The success of the ring imaging Cherenkov detector (RICH) concept [1] depends in no small measure on the performance of the photosensor. In 1990, solid CsI photocathodes were proposed for use in RICH detectors [2,3] as an alternative to the heated TMAE gas used in the largest RICH systems to date [4,5]. Since that time there has been some controversy as to the values of various parameters describing the performance of CsI photocathodes relevant to their use in RICH detectors. This paper reports the results from systematic studies that provide reliable values for these parameters.

A central issue concerns the quantum efficiency of CsI photocathodes. Measurements that used TMAE gas as a convenient reference show a factor of 2 variation in the apparent quantum efficiency, and one

report based on a supposedly calibrated photomultiplier indicated rather low quantum efficiency. However, good consistency in measurements of the quantum efficiency has been achieved by use of photodiodes calibrated by the US National Institute of Standards, as discussed in Section 2. The quantum efficiency of CsI is in the middle of the range of past measurements, and is somewhat smaller than that of TMAE gas.

The possibility of temperature dependence of the quantum efficiency of CsI is considered in Section 3. We find no temperature dependence for a fresh-made photocathode. However, some recovery of lost quantum efficiency is possible in an aged photocathode, or in one that has been exposed to water vapor.

The useful lifetime of a CsI photocathode is limited by charge-transport effects as discussed in Section 4. Studies reveal two aspects of the aging process: modification of the surface layer (i.e., a rise in the work function) due to both photoelectrons and positive ions, and change in the structure of the bulk CsI by

* Corresponding author. Tel. 609 258 6608, fax 609 258 6360, e-mail: mcdonald@puphep.princeton.edu.

photoionization. In practice the surface effect will determine the useful lifetime. We find that passage of photoelectrons across the surface causes aging 150 times as rapidly as does bombardment of the surface by positive ions (in case the photocathode is in a chamber with gas gain). For chambers with gas gain less than 150 the useful lifetime of the CsI photocathode will be about $0.1 \mu\text{C}/\text{mm}^2$, while for gas gains larger than 150 the useful lifetime will be about $15 \mu\text{C}/\text{mm}^2$. If the chamber has gain $\approx 10^5$ the lifetime of the CsI photocathode should be several decades at an e^+e^- B factory, but would only be a few years at a hadron collider with luminosity $10^{32} \text{ cm}^{-2} \text{ s}^{-1}$.

When a CsI photocathode is operated in a chamber with gas gain its quantum efficiency is always less than for operation under vacuum due to backscattering of photoelectrons in collisions with gas molecules. As discussed in Section 5, this effect depends on the strength of the electric field on the photocathode and on the gas pressure. Studies of the reduced electric field dependence of the quantum efficiency show that the penalty of using chambers with wire anodes at atmospheric gas pressure, rather than the more favorable case of mesh anodes under low gas pressure, will be the loss of about 8, 20 and 35% of quantum efficiency for methane, ethane and isobutane, respectively. Hence the use of atmospheric-pressure methane in chambers with wire anodes is indicated.

Finally, in Section 6 we report on the use of large anode-cathode separations to enhance charge sharing among cathode readout pads. Studies were made with a small RICH prototype equipped with a 32-channel readout system based on AMPLEX chips. The noise performance has reached the design goal, about 2000 electrons. The position resolution for single photoelectrons was measured to be better than 0.4 mm along with the anode wire direction, and 0.7 mm along with the direction perpendicular to the wire. This scheme will permit good spatial resolution to be maintained with large cathode pads, and hence a smaller channel count.

Results from a prototype RICH detector in a test beam are reported elsewhere [6].

2. Quantum efficiency of a CsI photocathode

Many measurements, including our own in the past [7], have been made using TMAE gas as the reference for absolute quantum efficiency. Such measurements are subject to systematic error due to poor purity of the TMAE, and due to unknown and variable amounts of TMAE adsorbed on chamber windows and walls during the measurements.

To make new measurements of the quantum efficiency of CsI that are not dependent on TMAE we

have obtained a calibrated CsTe photodiode from the National Institute of Standards (model 40560C) and also a CsTe photomultiplier (Hamamatsu model R1220) that has been calibrated by the vendor against a similar standard. We used a VUV monochromator (McPherson model 234/302) to check the vendor-supplied calibration curves in a setup as shown in Fig. 1.

First we installed the photodiode at the front port and the PMT at the side port. The VUV beam splitter was obtained from Acton Research, who provided calibration curves for its transmission and reflectance for the range 120–220 nm. A 1 mm diameter collimator in front of the beam splitter restricted the beam spot size. The collecting voltage of the photodiode was set at 150 V. For the photomultiplier, all of the dynodes and anode were connected together and the dynode collecting voltage set at 120 V. A Keithley model 617 electrometer was used to record the photocurrent. The monochromator was pumped down to be better than 10^{-3} Torr.

After we collected data with both the photodiode and PMT in this configuration, we interchanged the photodiode and PMT and scanned again. By this method we can check the consistency of three calibration curves: Q.E. of the photodiode, of the PMT, and the ratio of reflectance to transmission of the VUV beam splitter. We found the stated calibrations of the two photosensors to be consistent to within 10% over the wavelength range 120–220 nm, except in the region 150–160 nm where slightly higher deviations, $\sim 25\%$, were seen. The ratio of reflectance to transmission of the beam splitter also shows good agreement in shape with the vendor curve, but with normalization

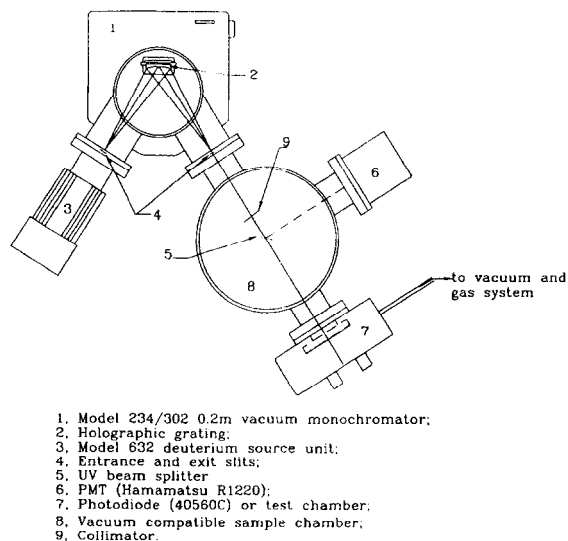


Fig. 1. Sketch of the VUV monochromator.

systematically shifted by 0.1. The results are shown in Figs. 2 and 3.

Having completed the calibration of photodiode, PMT and beam splitter, we installed the PMT at the side port and the test chamber containing a CsI photocathode at the front port. Our new results for the quantum efficiency of a CsI photocathode using the calibrated Hamamatsu R1220 photomultiplier as

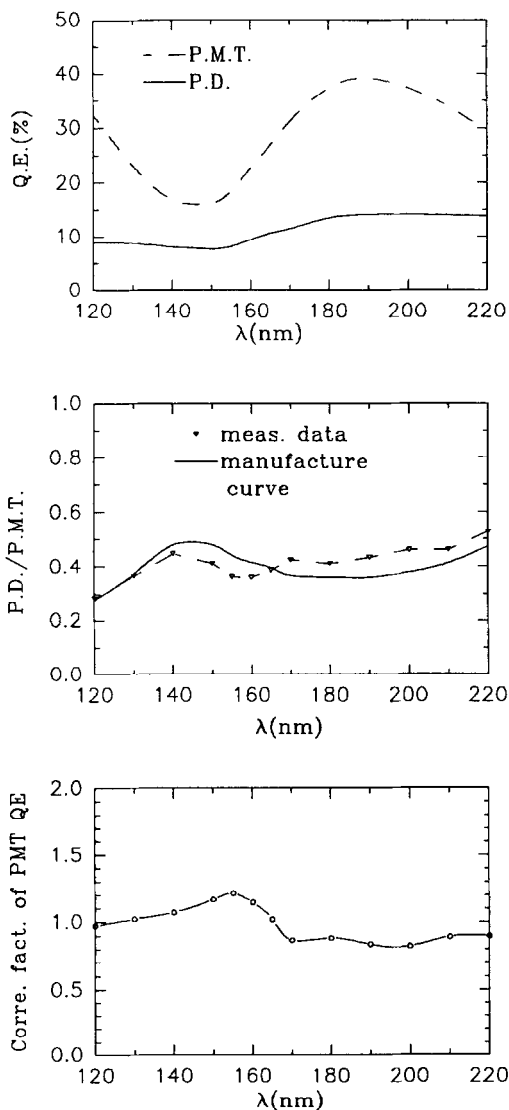


Fig. 2. Comparison of the quantum efficiency calibration of an NIST type 40560C photodiode and a Hamamatsu R1220 photomultiplier. (a) The quantum efficiency vs. wavelength of the two devices according to the manufacturers; (b) measured ratio of quantum efficiencies of the two devices compared to the ratio inferred from manufacturers specifications. (c) Correction factor of PMT Q.E.

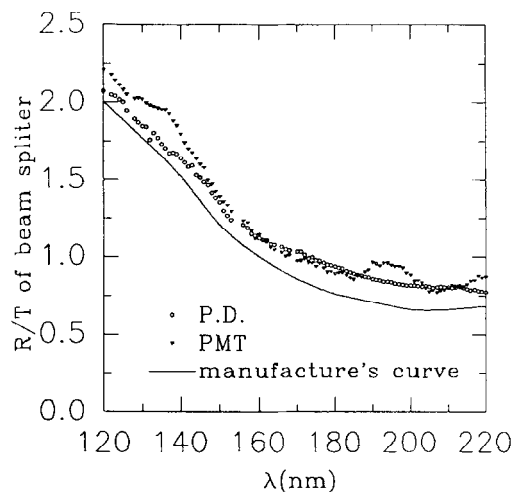


Fig. 3. Comparison of the measured reflectance/transmission of a VUV beam splitter to the manufacturer's data.

the reference are shown in Fig. 4. Also shown in the same figure are our previous results which used TMAE as the reference [7]. The older results are somewhat higher, likely due to uncorrected effects of TMAE adsorbed on the window of the previous test chamber.

The new corrected data of Breskin et al. [8] are also shown in Fig. 4, and our data appear to be very consistent with theirs.

We only show our data above 180 nm because we

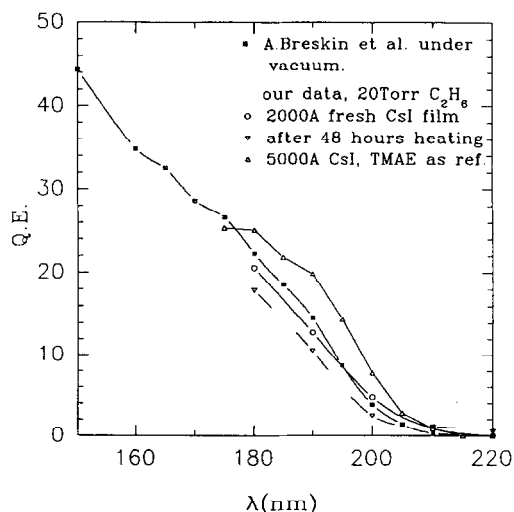


Fig. 4. Measured quantum efficiency of a CsI photocathode using a calibrated PMT as reference. Also shown are our older results using TMAE as reference [7], and results from Breskin et al. [8] using a calibrated PMT as reference.

measured the quantum efficiency in a chamber filled with ethane gas which absorbs UV light shorter than 170 nm [7]. Breskin et al. measured the quantum efficiency under vacuum.

3. Dependence of the quantum efficiency on temperature

There have been conjectures that the quantum efficiency of a solid CsI photocathode might be higher at higher temperature. The accumulated experience with other semiconductor photocathodes suggests that a strong temperature dependence is unlikely, and at least one null result has been reported for CsI [9].

Recently we have studied the temperature dependence of a CsI photocathode under vacuum. A deuterium lamp was used as the UV light source. Two diaphragm collimators defined the beam spot. The photocurrent was measured by Keithley 617 electrometer. The beam intensity was monitored via a beam splitter and an avalanche photodiode.

The experimental procedure was as follows: A CsI photocathode was evaporated (in vacuum) onto an aluminum substrate that was heated by illumination from an infrared lamp. The photocathode was then quickly transferred (in air) to the test chamber, which was pumped down immediately. To avoid possible aging of the CsI photocathode due to the relatively high intensity of the deuterium lamp, a shutter limited the illumination of the photocathode to brief intervals at each temperature. The temperature of the photocathode was varied by means of an electric heating pad on the back side of the aluminum substrate, and was measured by a thermocouple attached to the heating pad.

Results are shown in Fig. 5. There is no indication of a temperature enhancement of the quantum efficiency. Rather, when the temperature increased the quantum efficiency of the fresh-made photocathode actually decreased slightly.

However, we did observe a temperature dependence to the photocathode after large accumulated photocurrents, in qualitative agreement with an earlier report by Anderson et al. [11]. That is, an aged photocathode can regain some lost quantum efficiency if its temperature is raised. Our results are shown in Fig. 6, which shows a jump in photocurrent at points b and c when the temperature was raised after accumulation of several μC of collected charge.

In photoionization of CsI,



we believe that the neutral iodine atoms migrate out of the bulk CsI before the Cs^+ ions can be neutralized

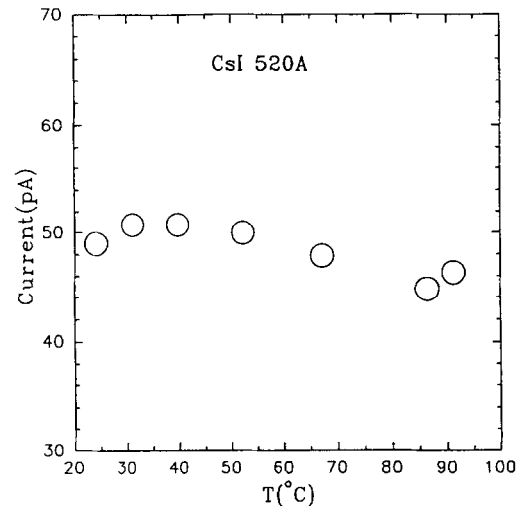


Fig. 5. Photocurrent vs. temperature for a fresh-made CsI photocathode on an aluminum substrate in vacuum.

by electrons from the substrate, since CsI is a poor conductor. Hence with time the surface of the CsI photocathode becomes partly Cs. This results in a lower quantum efficiency, but with some sensitivity at photon energies as low as 2 V, the work function of pure Cs. Heating the aged photocathode results in vaporization of the Cs atoms near the surface, which increases the proportion of CsI and partially restores the lost quantum efficiency.

More detailed studies of aging are reported in the next section.

We have also made measurements on a related issue: improvements in the quantum efficiency of CsI photocathodes by transient heating after exposure to water vapor [7]. In such a circumstance heating the

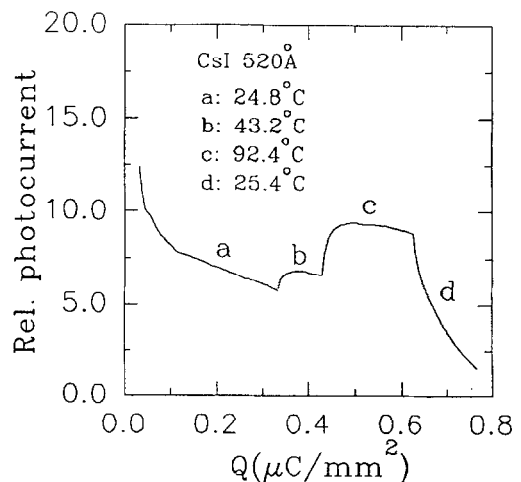


Fig. 6. The temperature dependence of photocurrent for an aged CsI photocathode in vacuum.

photocathode can help to get rid of the absorbed water vapor, and to recover the original quantum efficiency.

Any heating of chamber materials surrounding a CsI photocathode carries the risk of driving volatile chemicals onto the photocathode with attendant loss of quantum efficiency. Thus while transient heating of CsI photocathodes can have benefit, care must be exercised in the choice of chamber materials. If the photocathode is prepared with little exposure to water vapor there may be no need for transient heating, as appears to have been the case for the cathode reported in Fig. 4. In that figure we plotted the quantum efficiency of a fresh-made CsI photocathode as well as the same photocathode after being heated up for 45 h while the chamber is pumping down. The quantum efficiency is even lower after heating.

4. Aging of CsI photocathodes by charge transport

CsI photocathodes show a gradual loss of quantum efficiency with increased charge transport [10,11], as seen above in Fig. 6. This could be due to a bulk effect of ionization of CsI by light as discussed in Section 3, but also due to a surface effect in response to bombardment by positive ions from gas avalanches when the photocathode is operated in a gas-filled chamber. To separate these two effects we have made a series of measurements of aging of CsI photocathodes under vacuum and 20 Torr C_2H_6 with gas gains 300, 10^4 and 10^5 .

To study aging of CsI in vacuum a test chamber was illuminated by a collimated beam from a deuterium lamp. A Keithley model 617 electrometer was connected to the anode plane while the photocathode was held at -400 V. At various times the test chamber was removed from the beam of the deuterium lamp and installed on the VUV monochromator to determine its quantum efficiency as a function of wavelength. The results are shown in Fig. 7. The two glitches on the

photocurrent aging curve (a) at 0.2 and $0.6 \mu C/mm^2$ may indicate some recovery of quantum efficiency when we interrupted the intensive aging process to move the chamber to the monochromator.

There is a sharp decrease at the beginning of the aging process. After accumulating about $0.25 \mu C/mm^2$ the photocurrent drops to 70% of its initial value. Thereafter the aging rate becomes slower.

One layer of CsI consists of few $\times 10^{12}/mm^2$ CsI molecules, while $0.25 \mu C/mm^2$ corresponds to $\sim 10^{12}/cm^2$. This suggests that the sharp decrease in photocurrent at the beginning of the aging process is due to modification of the first layer of CsI molecules. The subsequent loss of quantum efficiency at a lower rate may be attributed to modification of the deeper layers of CsI by photoionization as discussed in the previous section.

Fig. 7b shows the wavelength dependency of aging process: CsI has a longer lifetime at shorter wavelengths. This effect is largely due to the aging during the first $0.25 \mu C/mm^2$ of charge transport during which the first layer of CsI is destroyed, apparently raising the work function.

When we performed this study, the deuterium lamp and the test chamber were separated by air. Photons with wavelength shorter than 190 nm were absorbed before hitting the photocathode, so the DC current aging curve (from Fig. 7a) is the average over the wavelength range of 190–220 nm, in agreement with the data in Fig. 7b.

We also studied the aging of CsI when the test chamber was filled with 20 Torr of ethane and operated at gas gains of 300, 10^4 , and 10^5 . The results are summarized in Fig. 8.

For the studies at a gas gain of 300 the setup was the same as above, so the air gap between the lamp and chamber absorbed the shorter-wavelength photons. Before and after an accumulation of $30 \mu C/mm^2$ charge we measured the quantum efficiency vs. wavelength by temporarily attaching the test chamber to the VUV monochromator. The data collected during

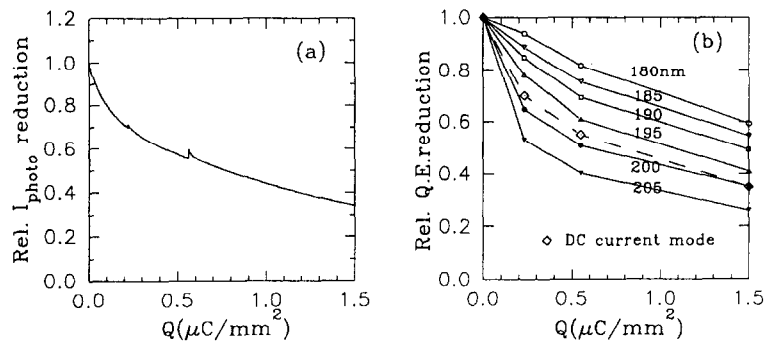


Fig. 7. The aging of a CsI photocathode in vacuum. (a) Photocurrent aging curve; (b) aging at different wavelengths.

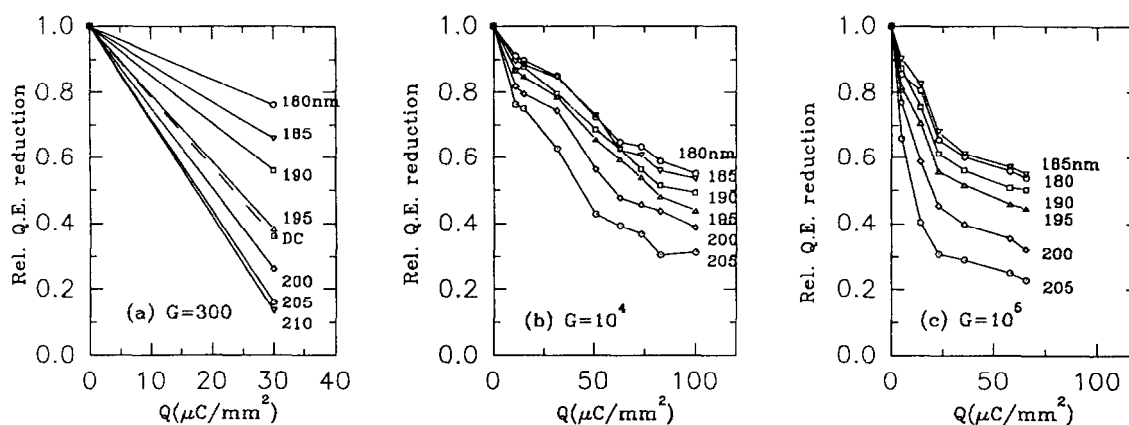


Fig. 8. The aging of a CsI photocathode in 20 Torr C_2H_6 . (a) Gas gain = 300; (b) gas gain = 10^4 ; (c) gas gain = 10^5 .

the aging process is shown as the dashed line labelled DC on Fig. 8a. The quantum efficiency fell roughly linearly with accumulated charge. We infer that the quantum efficiency at a specific wavelength also fell linearly with charge for the range studied, and connected the data points at 0 and $30 \mu C/mm^2$ with straight lines to guide the eye.

At gas gains of 10^4 and 10^5 , the photocurrents were large enough that the aging studies could be accomplished with the test chamber attached to the VUV monochromator. The wavelength was fixed at 180 nm during aging, but scans of quantum efficiency vs. wavelength were performed several times with results shown in Figs. 8b and 8c. When the studies were extended to collected charges of $100 \mu C/mm^2$ we observed a fast and slow component to the aging process, qualitatively similar to the case of unit gain (Fig. 7). The aging rate appears to increase somewhat at higher gas gain.

Again we interpret the fast component of the aging as due to modification of the surface layer, but now positive-ion bombardment from the gas plays a role as well as electron transport from the bulk CsI. The slow component of the aging remains, in our view, largely due to the change in composition of the bulk CsI material due to photoionization.

Because high values of the quantum efficiency are required for successful use of CsI photocathodes in a RICH detector, we consider the practical life of a CsI photocathode as that until the quantum efficiency has dropped to 80% of its initial value. From Figs. 7 and 8 we see that the fast component of the aging process is the critical one in this respect. It is therefore useful to model the fast component of aging in terms of coefficients k_p and k_i which represent the rates of aging due to photoionization and positive-ion bombardment, respectively. That is,

$$A_{\text{total}} = A_{\text{photon}} A_{\text{ion}} = e^{-k_p Q_p} e^{-k_i Q_i} = e^{-(k_p/G + k_i) Q_i},$$

where A is the relative quantum efficiency which decreases from initial value 1 due to aging, Q_p and $Q_i = GQ_p$ are the accumulated charges due to photoionization and positive-ion bombardment, respectively, and G is the gas gain. While the data may not support the hypothesis of exponential falloff of the quantum efficiency for large accumulated charges, exponential behavior is a reasonable description for this first 20% loss.

The data shown in Fig. 7 were collected with the chamber at vacuum, so $Q_i = 0$. We estimate that at $Q_p = 0.1 \mu C/mm^2$ the photocurrent dropped to 80%, using the average behavior shown in Fig. 7a (also labelled as DC current mode in Fig. 7b). Therefore $e^{-0.1k_p} = 0.8$ and $k_p = 2.2 \text{ mm}^2/\mu C$. For the test with gas gain of 300, the average behavior labelled DC in Fig. 8a shows that at $Q_i = 10 \mu C/mm^2$ the quantum efficiency drops to 80%. Hence $e^{-10(k_p/G + k_i)} = 0.8$, and $k_i = 0.015 \text{ mm}^2/\mu C \approx k_p/150$. That is, the aging effect due to photoelectron transport across the CsI surface is 150 times stronger per unit charge than that due to positive-ion bombardment.

The result that $k_i \approx k_p/150$ indicates that for gas gain which is large compared to 150 the fast component of aging is dominated by positive-ion bombardment, and that the accumulated charge for, say, 20% loss of quantum efficiency is about $15 \mu C/mm^2$ independent of the gas gain. The latter prediction is supported by the data shown in Figs. 8b and 8c for gas gas gains of 10^4 and 10^5 , taking the results at 195 nm as representative of the average behavior of the quantum efficiency.

We conclude this section by casting the effective lifetime of $10 \mu C/mm^2$ of a CsI photocathode into other units. This value is equivalent to 10^{14} unit charges/ mm^2 . For a gas gain of, say, 10^5 , the lifetime is then 10^9 photoelectrons/ mm^2 . Supposing the RICH detector achieves a sensitivity of 10 photoelectrons per particle in the 1–4 GeV range, the detector life would

be 10^8 particles/mm². A central barrel RICH detector would have about 30 m² of active area, so the lifetime of the whole detector would be about 3×10^{15} particles. If we desire a detector life of 10 physics years = 10^8 s, the particle flux through the RICH detector must be less than 3×10^7 /s. Such a high flux is unlikely to be encountered at an e^+e^- collider, but is roughly the expected rate at a hadron collider operating at luminosity 10^{32} cm⁻² s⁻¹.

5. Electric field dependence of the quantum efficiency

The quantum efficiency of a CsI photocathode in a gas-filled chamber will in general be less than that for a chamber in vacuum because some photoelectrons will be backscattered onto the cathode by collisions with gas molecules [12]. However, an electric field on the photocathode can accelerate the photoelectrons to high enough energies before molecular collisions that the backscatter cross section is greatly reduced. High fields on the photocathode and low molecular collisions rates might be best achieved in chambers with mesh anodes that are operated at low pressure. However, there are (at least) two salient reasons to prefer the use of anode wire planes instead of anode mesh planes:

- Chambers with wire anodes will be able to operate at atmospheric pressure with pure organic gases such as methane, ethane and isobutane. A parallel-plate avalanche chamber (PPAC) with a mesh anode can operate only at low pressure with these gases. A PPAC can operate with atmospheric-pressure helium gas mixtures, but the penalty is lower quantum efficiency of the photocathode due to scattering of photoelectrons back onto the cathode [13].
- According to the in-beam experience of CERES UV detectors [14] a PPAC configuration is more vulnerable to the sparking due to the fast breakdown occurring at a total charge of 10^8 electrons in an avalanche. Such large avalanches are due to nuclear

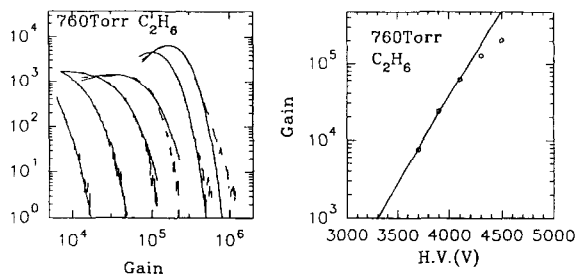


Fig. 10. Induced-charge spectra on one central cathode pad in a RICH prototype with MWPC configuration. (a) Charge spectra; (b) gain vs. high voltage.

interactions near the surface of chamber materials. In an anode wire configuration the avalanche size is self-suppressed because of space-charge effects if the avalanche is larger than 10^6 electrons, and the probability of sparking is greatly reduced.

Since the electric field at the cathode plane is quite different when using an anode wire mesh and anode wire plane, it is useful to understand the dependence of the quantum efficiency on the chamber configuration. This issue has also been considered by Anderson et al. [15] and Breskin et al. [16].

We have made recent studies of the electric field dependence of the quantum efficiency of CsI by adding an anode wire plane and a cathode mesh plane to a small RICH prototype that was previously used in tests at BNL [17]. A sketch of the chamber is shown in Fig. 9.

After an anode wire plane and a cathode mesh plane were installed in the prototype chamber, we operated it with atmospheric-pressure methane, ethane and isobutane. Typical gas gain spectra of single-photoelectron-initiated gas avalanches, together with the gas gain vs. high voltage, are shown in Fig. 10. The single-pad gain shown in Fig. 10 should be multiplied by a factor 2.74 to obtain the total gain; this includes a factor of 2 since there are two cathode planes, and a factor of 1.37 as the ratio of the charge on one plane to the charge induced on the central pad.

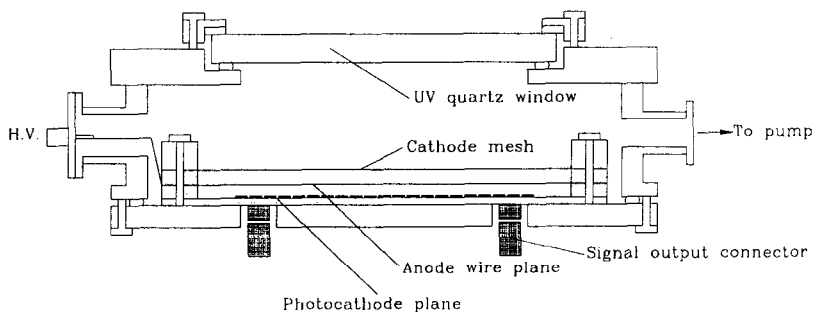


Fig. 9. A RICH prototype with an anode wire plane.

In Fig. 10b we show the results for ethane gas; methane and isobutane were also studied and have similar behaviours. For six different pressure of ethane gas (760, 376, 200, 94, 49, and 20 Torr) the charge spectra were collected. Because the shapes of those spectra are different the threshold effects are different. To compensate for the lost part of the spectra below the threshold each spectrum is fitted with a Polya distribution, and the number of events below the threshold of fitted Polya curve are added to the integral of the observed spectrum to get a total quantum efficiency.

The electric field at the cathode can be calculated from Ref. [18]:

$$E_y \approx \frac{2\pi V_0}{2\pi d/s - 2 \ln(\pi D/s)}, \quad d > s,$$

where E_y is the electric field along the y -direction, which is perpendicular to the anode wire plane, d is the distance between anode and cathode planes, s is the anode wire pitch, D is the anode wire diameter, and V_0 is the high voltage on the anode wire. Using this expression the data of Fig. 10 were reinterpreted as the relative quantum efficiency vs. the reduced electric field (E/P) at the photocathode, with results as shown in Fig. 11 for methane, ethane, and isobutane. The six different values of E/P for each gas represent six different pressures between 760 and 20 Torr. We found that a reduction in relative quantum efficiency of 8, 20 and 35% at 760 Torr compared with 20 Torr for methane, ethane, and isobutane, respectively.

These results contrast with that for CsI under vacuum, where Bräuning et al. found no (or very little)

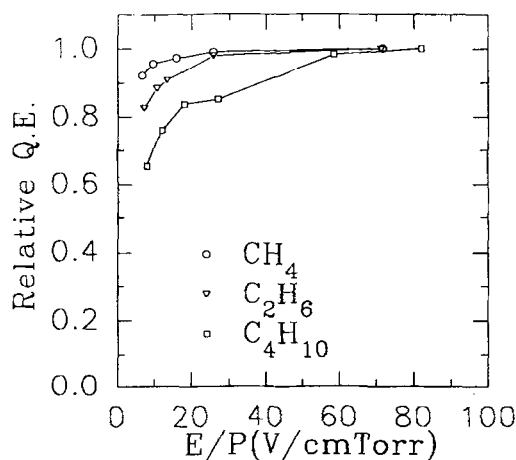


Fig. 11. The dependence of the quantum efficiency on the reduced electric field, E/P , in methane, ethane, and isobutane.

electric field dependence of the quantum efficiency over the range of 50–2000 V/mm [9]. This null result is expected since the mean free path length for photoelectrons in solid CsI is only a few nm [7]. Hence for any influence on the electron extraction from the CsI, the electric field should be around 1 V/nm, which is several orders of magnitude higher than the applied electric fields of ~ 1 kV/mm.

Our results on electric field effects on the quantum efficiency of CsI photocathodes in gas media are quite consistent with those of the Breskin group [16] who found a Q.E. reduction in gases of about 3% for methane, $\sim 20\%$ for ethane, and $\sim 30\%$ for isobutane, compared to vacuum. We concur with their conclusion that the Q.E. of a CsI surface in gas is always lower than in vacuum due to the backscattering of photoelectrons from gas molecules. For high values of the reduced electric field the gas avalanche starts close to the photocathode, so the probability for elastic scattering decreases due to the opening of new inelastic channels in the electron–molecule collisions. When the probability of the elastic collisions drops to zero, the Q.E. in the gases must reach the vacuum value.

We have measured the reduced Townsend coefficient α/P of ethane and isobutane [13]. From fits to the data of the form $\alpha/P = a + bE/P$, we derived the minimum reduced electric field required to start the gas avalanche, $(E/P)_{\min}$, which is 56.1 V/cm Torr for ethane, and 89.9 V/cm Torr for isobutane. Such high reduced electric fields at the cathode can only be reached under low gas pressure, and hence only for CsI photocathodes in low-pressure gas chambers will the Q.E. be close to the vacuum value.

6. Charge sharing on cathode readout pads

The reconstruction of Cherenkov rings in RICH detectors with dimensions appropriate for central B physics requires spatial resolution of about 1–2 mm. Finer resolution is not warranted because of limitations of chromatic aberration in the radiator, and because of broadening of the ring due to the finite thickness of the radiator in the case of proximity focusing. This has led to a specification of readout pad size of typically 8×8 mm, and correspondingly a channel count of about 600k for a detector of 40 m^2 surface area.

If the anode–cathode spacing is increased, the image charge on the cathode pads will be smeared over multiple pads and good spatial resolution could be obtained by charge sharing among coarser pads [19]. The spatial distribution $\rho(x)$ of the image charge is governed by the chamber gap, called d in Fig. 12, according to [20]

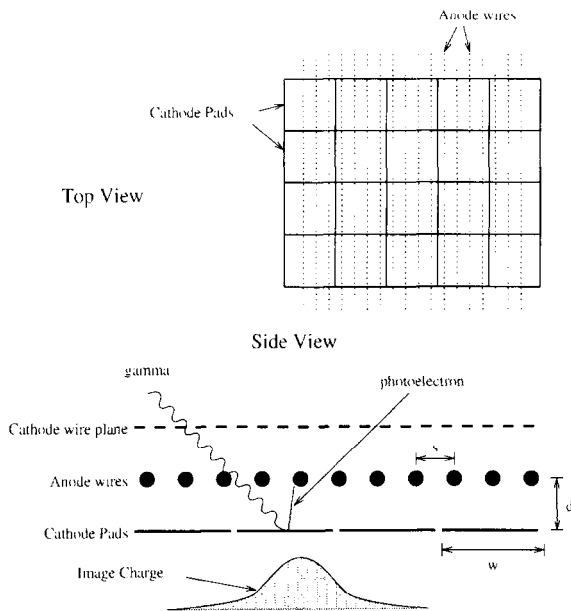


Fig. 12. Design of a RICH photodetector with a CsI photocathode segmented into pads of width w separated by a gap d from the anode plane consisting of wires of spacing s .

$$\rho(x) = \frac{\pi}{8} \operatorname{sech}^2\left(\frac{\pi x}{2d}\right).$$

The reconstructed location of a photoelectron is obtained by simple charge weighting of the struck-pad coordinates. An estimate for the position resolution that can be obtained for single-photoelectron events detected using a 3×3 array of square pads is

$$\frac{\sigma_x}{w} = \frac{\sqrt{6}\sigma_Q}{0.45\bar{G}},$$

where σ_Q is the electronic noise on a single pad, and w is the pad width. The factor 0.45 reflects the portion of the charge in the avalanche that is imaged onto the readout cathode. For $8 \times 8 \text{ mm}^2$ pads and an average chamber gain of $\bar{G} = 1.0 \times 10^5$ this yields a resolution slightly better than 1 mm.

6.1. Induced charged distribution on a “pseudostrip”

To test the charge-sharing idea, we have installed the RICH prototype (Fig. 9) vertically on an x - y stage and perpendicular to the light beam of our VUV monochromator. The window of the prototype chamber was directly against the output window of the monochromator to minimize the air gap and consequent absorption of UV light.

In the initial studies we could only analyze a single channel via an EG&G Ortec model 142PC preamplifier. Therefore three consecutive horizontal pads

were connected together to form a “pseudostrip”, the induced charge on which for single photoelectrons was observed for several vertical positions of the chamber relative to the light source, with results shown in Fig. 13. The solid line in Fig. 13 is derived by integrating the theoretical charge-distribution given above to take into account the finite strip widths. The observed distributions match the theoretical curve very well.

6.2. Position resolution via charge sharing

For a second round of studies we used a 32-channel prototype of a readout electronics system based on AMPLEX chips [21]. The AMPLEX chips provide charge integration and pulse shaping ($\sim 750 \text{ ns}$) as well as a sample-and-hold subcircuit. A total of 16 channels are available in each chip. The circuit board was designed to interface directly with the RICH prototype. The AMPLEX chips were controlled by a LeCroy model 2366 Xilinx CAMAC module that was interfaced to an IBM PC. The overall functional block diagram is shown in Fig. 14. With the AMPLEX circuit board connected to the RICH prototype the typical σ_{noise} was measured to be ~ 2000 electrons, and the overall gain was ~ 235 electrons/ADC count.

The prototype RICH chamber with the 32-channel readout was then used in the configuration shown in Fig. 15. A hydrogen lamp emitted 1 ns wide pulses of UV light at a rate of about 1 kHz. These pulses were collimated by a pair of 0.5 mm wide slits before impinging on the prototype chamber, which could be moved transversely on an x - y stage. In this way the

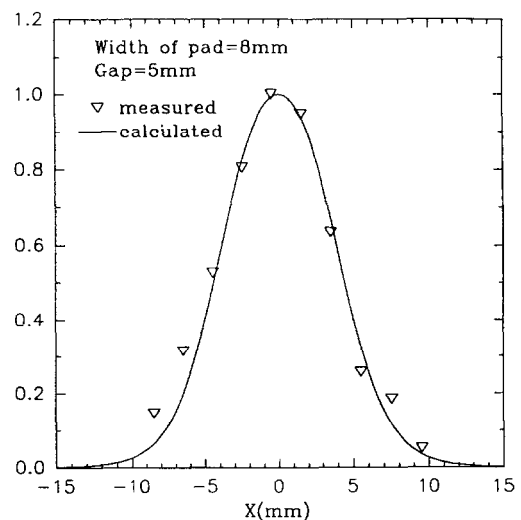


Fig. 13. The distribution of induced charge on an 8 mm wide “pseudostrip” vs. the distance from the center of the strip to the center of the gas avalanche.

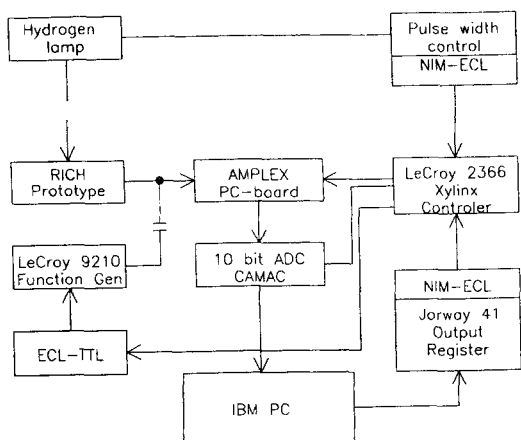


Fig. 14. Block diagram of the AMPLEX readout system.

location of the UV light on the chamber was known to better than 0.2 mm.

The output of the hydrogen lamp was attenuated by neutral density filters until a signal was observed in only one pulse in ten, insuring a 90% probability for single photoelectrons. The location of the photoelectron was reconstructed by a simple weighting of the stuck-pad coordinates by the induced charge observed on the pad by the AMPLEX chips. Plots of true position vs. measured position are shown in Fig. 16.

For the y direction (parallel to the anode wires) the correlation between true and reconstructed position is excellent. In contrast, for the x direction (perpendicular to the anode wires) the effect of the 2.5 mm anode wire spacing is evident. The rms position resolution in y is typically $\sigma_y = 0.35$ mm. This is about 40% larger than what would be expected from the

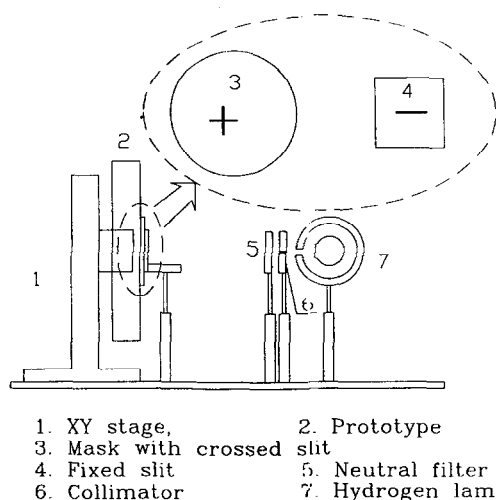


Fig. 15. A sketch of the setup used to measure the position resolution in a 32-channel prototype RICH detector.

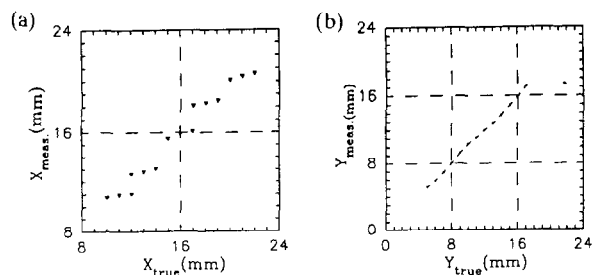


Fig. 16. True position vs. reconstructed position in the prototype RICH detector. (a) x direction (perpendicular to the anode wires); (b) y direction (parallel to the anode wires).

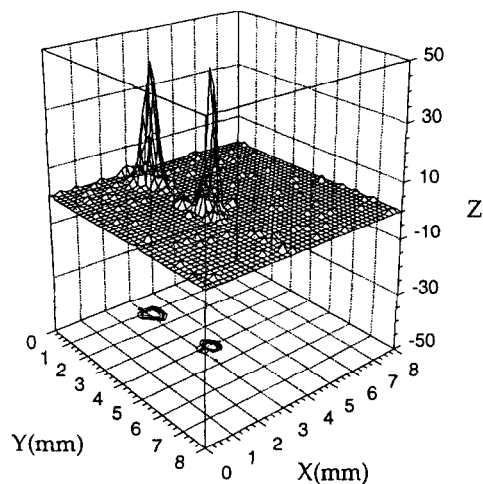


Fig. 17. 3D image of the reconstructed x - y position distribution in the prototype RICH detector.

simple estimate made above. The difference probably results from the non-negligible fraction of single-photoelectron events with gas gains much smaller than \bar{G} .

In the x direction the position resolution should be $1/\sqrt{12}$ times the wire pitch, namely $\sigma_x = 0.73$ mm for our case of 2.54 mm wire spacing.

A 3D plot of the distribution of reconstructed x - y positions is shown in Fig. 17, in which the data collected for two positions of the chamber 3 mm apart have been superimposed.

References

- [1] J. Séguinot and T. Ypsilantis, Nucl. Instr. and Meth. 142 (1977) 377.
- [2] V. Dangendorf et al., Nucl. Instr. and Meth. A 289 (1990) 322.
- [3] J. Séguinot et al., Nucl. Instr. and Meth. A 297 (1990) 133.

- [4] D.W.G.S. Leith, *Nucl. Instr. and Meth. A* 265 (1988) 120.
- [5] R. Arnold et al., *Nucl. Instr. and Meth. A* 270 (1988) 255 and 289.
- [6] C. Lu et al., Prototype Studies of a Fast RICH Detector with a CsI Photocathode, submitted to *Nucl. Instr. and Meth.*
- [7] C. Lu and K.T. McDonald, *Nucl. Instr. and Meth. A* 343 (1994) 135.
- [8] A. Breskin et al., *Nucl. Instr. and Meth. A* 343 (1994) 159.
- [9] H. Bräuning et al., *Nucl. Instr. and Meth. A* 327 (1993) 369.
- [10] V. Dangendorf et al., *Nucl. Instr. and Meth. A* 308 (1991) 519.
- [11] D.F. Anderson et al., *Nucl. Instr. and Meth. A* 323 (1992) 626.
- [12] D.F. Anderson et al., *Nucl. Instr. and Meth.* 217 (1983) 217.
- [13] C. Lu, K.T. McDonald and Y. Zhu, *Nucl. Instr. and Meth. A* 334 (1993) 328.
- [14] R. Baur et al., *Nucl. Instr. and Meth. A* 343 (1994) 231.
- [15] D.F. Anderson, S. Kwan and V. Peskov, *Nucl. Instr. and Meth. A* 343 (1994) 109.
- [16] A. Breskin et al., WIS-93/115/Dec.-PH.
- [17] N.S. Lockyer et al., *Nucl. Instr. and Meth. A* 332 (1993) 142.
- [18] G.A. Erskine, *Nucl. Instr. and Meth.* 105 (1972) 565.
- [19] E. Prebys, Proposal for a wire chamber-based CsI photocathode for a B-Factory RICH, Princeton U. preprint (Jan. 1994).
- [20] E. Mathieson and J.S. Gordon, *Nucl. Instr. and Meth.* 227 (1984) 277.
- [21] R. Wixted, An AMPLEX based RICH detector readout, preliminary test setup documentation, Princeton Internal Report (28 March, 1994).